Electronic properties of metallic Hg monolayers on W (110)

1994 J. Phys.: Condens. Matter 6 33

(http://iopscience.iop.org/0953-8984/6/1/006)

J. Phys.: Condens. Matter 6 (1994) 33–54. Printed in the UK

Electronic properties of metallic Hg monolayers on W(110)

Jiandi Zhang†‡, Dongqi Li†§ and P A Dowben†‡

† Department of Physics, Syracuse University, Syracuse, NY 13244-1130, USA
‡ Department of Physics, University of Nebraska–Lincoln, Lincoln, NE 68588-0111, USA
§ Materials Science Division, Building. 223, Argonne National Laboratory, Argonne, IL 60439, USA

Received 13 August 1993, in final form 4 November 1993

Abstract. The evolution of the electronic structure of ultrathin mercury layers on tungsten(110) with increasing thickness was studied by angle-resolved and resonant photoemission. There is evidence for the formation of new Hg electronic states arising from Hg adatom hybridization and quantum-well states. These results, combined with the resonant photoemission, suggest that the overlayer undergoes a gradual non-metal-to-metal transition with increasing coverage and are similar to the change of the metallic properties observed in free Hg clusters with increasing size. The Hg band structure exhibits little evidence for strong interactions or hybridization with the W(110) substrate, in spite of layer by layer growth of the Hg overlayer, and superlattice periodicity.

1. Introduction

Within the last several years, there have been an increasing number of experimental examples demonstrating that ultrathin overlayers of materials normally considered to be metals exhibit non-metal character on a metal substrate [1–11]. Typically, these systems exhibit a non-metal-to-metal transition with changing film density, structure or film thickness [10 11]. The surprise has been that this behaviour seems to occur for metal films on metal substrates not only for metals on semiconductors [12–22]. Among the several metal overlayers exhibiting a non-metal-to-metal transition on metal surfaces include overlayers of mercury [1–4], barium [3, 5–7], strontium [6], magnesium [6], thallium [8], and lithium [9].

According to the scheme of Miedema and Dorleijn [23] for divalent metals and the theoretical calculations of the monolayer [24], the non-metal-to-metal transition can be related to the coordination numbers of Hg. Essential to this model of a non-metallic overlayer on a metal substrate is an implicit assumption that the substrate overlayer interaction is weak. For most Hg overlayers, this is certainly clear [25–27]. In the case of Hg on tungsten(110), islanding appears to occur and a gradual increase in metallicity has been postulated for increasing island size [1]. This transition resembles the non-metal-to-metal transition in free Hg clusters that occurs with increasing cluster size [28–32]. In this paper, we report our systematic studies of the evolution of the electronic structure of the Hg overlayer and the gradual non-metal-to-metal transition of Hg overlayers on the W(110) surface. The incommensurate Hg overlayer exhibits a two-dimensional band structure only weakly influenced by the substrate.

0953-8984/94/010033+22$07.50

2. Experimental details

The experiments were carried out in a UHV system equipped with a hemispherical analyser, and a retarding-field analyser for LEED described previously [33]. The light source for the photoemission studies was dispersed by a 1 GeV ring at the Synchrotron Radiation Center. The incidence angle of the light is defined with respect to the surface normal. The incident light, 36° or 65° off normal, was used to give larger portion of light with its vector potential parallel to or perpendicular to the surface (s or p polarization, respectively). In the angle-resolved photoemission, the analyser was used to collect the photoelectrons in the plane parallel to the plane defined by the surface normal and the surface component of the vector potential $\boldsymbol{A}$, i.e., $\boldsymbol{K}_{11}$ is along $\overline{\Gamma N}$ direction of surface Brillouin zone of W(110), or perpendicular to the surface component of the vector potential $\boldsymbol{A}$, i.e., $\boldsymbol{K}_{11}$ is along the $\overline{\Gamma H}$ direction of the surface Brillouin zone of W(110). The energy analyser has an acceptance angle of $\pm 1.0°$ and the energy resolution of the photoemission spectra, including the light source, varied from 0.12 to 0.2 eV, (full width at half maximum). Relative photoemission intensities were determined from the integral counts for a photoemission feature, normalized by the synchrotron electron beam current and the flux transmitted through the monochromator. The binding energies of the photoemission features are referred to the Fermi level. The partial photoemission cross-sections of constant-initial-state (CIS) spectra were carried out as described elsewhere [3, 4]. The kinetic energy and photon energy were changed simultaneously, so as to determine the relative photoemission intensity of a given initial state. The CIS spectra were normalized for photon flux through the monochromator using the current from a gold diode at the exit of the monochromator. Several different initial states were examined to eliminate effects resulting from Auger electron features and second order light effects in the CIS spectra.

The W(110) substrate was cleaned by the accepted procedure of annealing in ambient O_2 and flashing [34]. Following cleaning, the crystal was cooled to 200 K with the use of a liquid-nitrogen cold stage (as determined with a W–5% Re/W–26% Re thermocouple). The Hg adsorption was undertaken with techniques described elsewhere [35]. The base pressure was about 7×10^{-11} torr. The ambient Hg pressure during the adsorption was always less than 2×10^{-8} torr.

3. Growth and formation of the Hg overlayer

The Hg adsorbs readily on W(110) at 200 K. The development of the Hg-induced photoemission features and the attenuation of the W(110) photoemission features at normal emission, with increasing Hg exposure, are shown in figure 1. With increasing exposure all the W(110) photoemission features become suppressed, while two intense features attributable to the Hg 5d spin–orbit doublet appear at binding energies of 9.8±0.1 eV ($5d_{3/2}$) and 7.8±0.1 eV ($5d_{5/2}$). The adsorption curve as determined by the Hg 5d and the W 4f photoemission signals is shown in figure 2(a). The slope in the ratio of the Hg 5d intensities relative to the W 4f intensity increases with increasing Hg exposure as seen in figure 2(b). Since any three-dimensional island formation or amalgamation of the Hg would result in an Hg-to-W signal ratio that changed little with increasing Hg exposure after a small initial exposure, the data suggest that the layer by layer growth dominates the adsorption process in the coverage range up to several monolayers. From the attenuation of the W 4f signal we estimate that the first layer of Hg is established after 4–5 L exposure, and a complete close packed layer is formed at 8 L. The adsorption of the second layer

results in the 'kink' in the adsorption curves (seen in figure 2). These results are generally consistent with previous studies of Hg on W(110) [36]. Layer-by-layer growth has been observed for Hg on Ag(100) [25, 37, 35] and Cu [25, 37, 38].

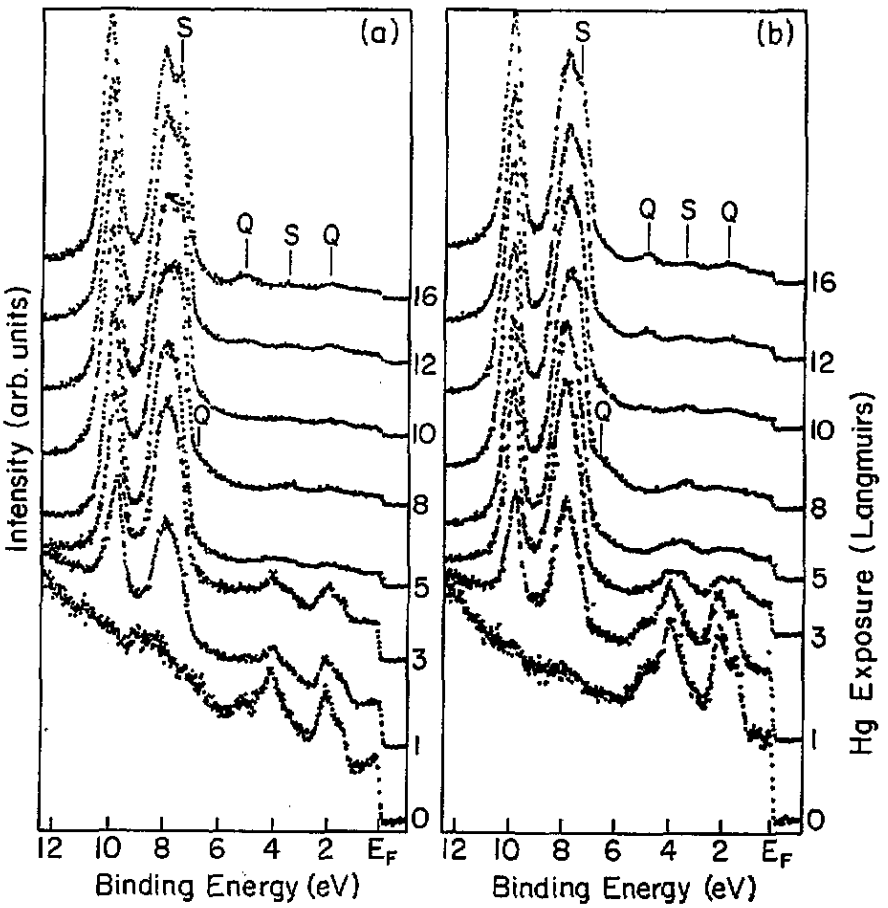

Figure 1. The photoemission spectra for Hg on W(110) at 200 K with increasing Hg exposure. The photoelectrons were collected normal to the surface. The light incidence angles are 36° (s polarized) (a) and 65° (p polarized) (b). The Hg quantum-well states are indicated by Q and the additional Hg overlayer band structure related states by S. The photon energy used was 40 eV.

Using the Hg-to-W intensity ratios (figure 2(b)) and supposing that the thickness of one Hg monolayer is 3.0 Å, we found that the electron mean free path through Hg is about 5.54 Å for an electron kinetic energy of about 25–28 eV. If we use the empirical mean-free-path formula [39],

$$\lambda = \frac{\varepsilon}{a(\ln \varepsilon + b)} \tag{1}$$

for the electrons with kinetic energy ε=25 eV in the Hg layer ($a = 14.5$, $b = -2.7$ [39]), then the mean free path is only about 3.32 Å. The reason for the difference between these two

results is that this simple empirical theory is not strictly valid for such low-kinetic-energy electrons.

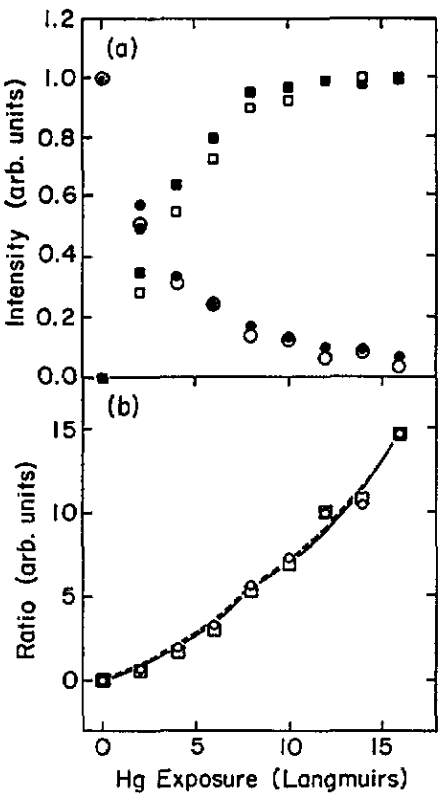

Figure 2. The Hg adsorption curve on W(110) at 200 K. The photoemission intensity changes of Hg $5d_{3/2}$ and $5d_{5/2}$, W $4f_{5/2}$ and $4f_{7/2}$, are shown in (a). The ratios of intensities of Hg $5d_{3/2}$(□) and $5d_{5/2}$(○) to W $4f_{7/2}$ are shown in (b). Data for several experiments are shown.

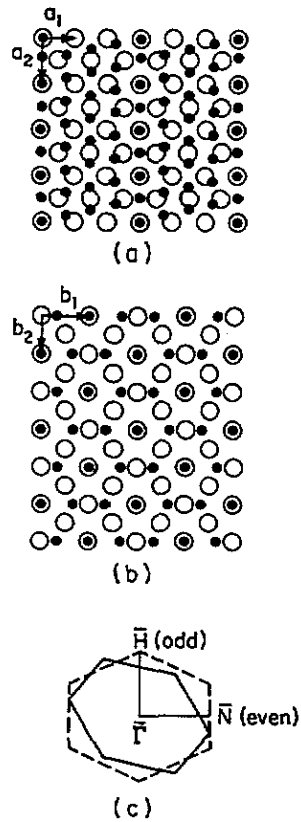

Figure 3. The schematic representation of the observed reciprocal space pattern of the Hg overlayer (●) on W(110) (○) (a) and the corresponding structure in real space (b). The overlayer and W(110) surface Brillouin zones are shown in (c).

For W(110) at room temperature, exposure to Hg does not result in any Hg-induced features appearing in the valence band photoemission even for exposures as large as 15–20 langmuirs (1 langmuir = 1×10^{-6} torr s). This suggests that the surface bonding between Hg atoms and W(110) is weak, indeed weaker than is observed for Hg on W(100) [26].

For adsorption of Hg on W(110) at 200 K, only one LEED pattern was observed for different Hg exposures up to two monolayers or more than 16 langmuirs. The schematic LEED pattern and one possible corresponding real-space structure are shown in figure 3(a) and (b), respectively. Using the conventional matrix notation of the LEED [40], we can describe the overlayer lattice net in terms of the substrate lattice net in real space by $\mathbf{B} = \mathbf{GA}$, where $\mathbf{B}$ is the overlayer lattice matrix, $\mathbf{A}$ the substrate lattice one and $\mathbf{G}$ a transformation matrix. The correspondence in the reciprocal space is described by $\mathbf{B}^* = \mathbf{G}^{\dagger}\mathbf{A}^*$. Using the choice

of reciprocal- and real-space vectors indicated in figure 3, we can write the matrix

$$\mathbf{G}^{\dagger} = \begin{pmatrix} \frac{3}{2} & \frac{3}{4} \\ 0 & 1 \end{pmatrix}$$

to describe the LEED pattern. For the real space we have

$$\mathbf{G} = \begin{pmatrix} \frac{2}{3} & 0 \\ -\frac{1}{2} & 1 \end{pmatrix}$$

to describe the real space overlayer lattice. There are two domains of this structure which are symmetric to each other along the substrate $\langle 1\bar{1}0 \rangle$ direction. Both domains contribute to the LEED pattern. From the LEED and this postulated interpretation for the corresponding real-space structure, it is clear that the Hg overlayer has a quasihexagonal structure and does not change its phase with increasing coverage up to two monolayers. For this ordered thin film, the Hg–Hg lattice constants are 2.98 Å and 3.49 Å along the substrate $\langle 001 \rangle$ and $\langle 111 \rangle$ directions, respectively. The unique Brillouin zone, as shown in figure 3(c), is consistent with our experimental band structure dispersion data as will be discussed below. This overlayer structure is also consistent with our assignment of submonolayer growth to two dimensional island formation [1].

Accepting this structure as the one-monolayer close-packed lattice, it is clear that the sticking coefficient for Hg on Cu(100) differs slightly from that for Hg on W(110) at 200 K even though both surfaces exhibit layer-by-layer growth. A close-packed monolayer (9.6×10^{18} atoms m^{-2}) is completed on Cu(100) at 200 K by 11 langmuirs [25, 37, 3] while for Hg on W(110) at 200 K a close-packed layer (1.06×10^{19} Hg atoms m^{-2}) occurs at about 8 langmuirs, suggesting that the sticking coefficient of Hg on W(110) is one and half times that on Cu(100).

4. The hybridization between the overlayer and substrate

The work function was measured from the emission threshold in photoemission as a function of coverage and is plotted in figure 4. The initial work function decreases almost linearly from 5.06±0.05 eV (which is close to the intrinsic work function of the W(110) surface [3, 9]) and then the reaches a shallow minimum (ϕ_{min}=4.4 eV, $-\Delta\phi_m$=0.66 eV) at about 9 langmuirs(ϑ_m). The work function minimum occurs at a coverage close to the coverage corresponding to one monolayer. By about two monolayers (16 L), the work function of bulk Hg is adopted.

Given the very small work function change ($-\Delta\phi_m$=0.66 eV, corresponding to very small induced dipole moment at the initial adsorption of 0.044e Å), and insignificant W(4f) binding-energy shift of less than 0.1 eV, it is clear that there is little charge transfer between the Hg adatoms and the substrate. While the intensities of the W(110) photoemission features are largely attenuated for Hg coverages beyond half a monolayer, the binding energies of the W(110) photoemission features are unaffected by the Hg overlayer. Not surprisingly, the W(110) 2.05±0.1 eV and 4.05±0.1 eV bulk valence-band features do not alter in binding energy with Hg adsorption. Only the W(110) surface states are seen to be affected by Hg adsorption, and this effect is slight. With increasing Hg coverage, the

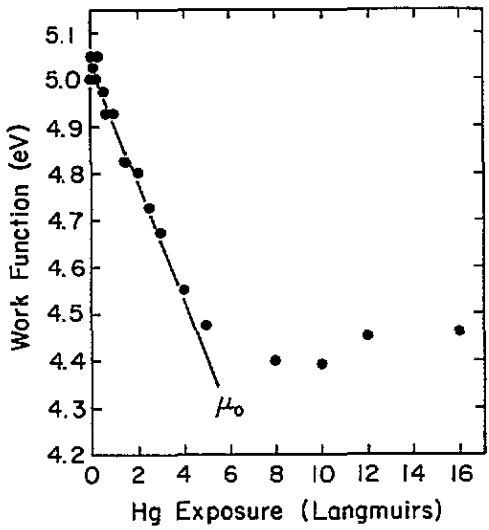

Figure 4. The work-function change, $\Delta\phi$, versus Hg coverage (and exposure) on W(110) at 200 K. The best-fit result for the initial dipole moment (solid line) is also represented.

W(110) surface state just below the Fermi energy shifts by about 200 meV to higher binding energy from 0.4±0.1 eV for the clean surface (as seen from figure 5), and attenuates evenly. This state is one of the W 5d surface states with d_{z^2} character [41]. The adsorbate-induced binding-energy shifts of this kind of surface state have been observed in many other systems, such as Hg/W(100) [42], Cs/W(100) [43], Cs/Ta(100) [43], Cs/Mo(100) [43] and Cs/Cu(111) [44]. According to Wimmer *et al* [45] and Soukiassian *et al* [43], the electronic origin of the shifts can be understood by the formation of covalent bonds between the d-like surface state of the substrate and the s-derived valence states of adsorbate. When the adatoms are adsorbed on the surface, the surface state forms polarized covalent bonds with the adatom 6s-derived state. As a result, the binding energy of the hybridized bonding state is higher than that of the surface state on a clean surface. The magnitude of the binding-energy change should be proportional to the strength of the surface bonding. Comparing with the shift of the W surface states with alkali or other metal deposition [43], the small shift (only about 0.2 eV compared with the 1.0 eV shift observed for the W d_{z^2} surface state in Cs/W(100) system) of the surface state with Hg adsorption is consistent with our postulate that the adlayer bonds weakly with the substrate. The core level binding energies and work function indicate little charge transfer, and, as noted above, Hg desorbs from W(110) below room temperature. We conclude that there is little hybridization of the Hg-overlayer electronic states with the W(110) states.

5. Development of the Hg 5d overlayer band structure

As seen in figure 1, the two dominant features induced by Hg adsorption are the Hg 5d spin–orbit doublet, increasing intensity with increasing coverage. The half width of both 5d doublet features also increases with exposure (as indicated in figure 6) until one Hg monolayer is reached. In the envelope of the Hg $5d_{5/2}$ feature a second $5d_{5/2}$ feature at about 7.2 ± 0.1 eV can be seen after about half a monolayer (4 langmuirs exposure), and

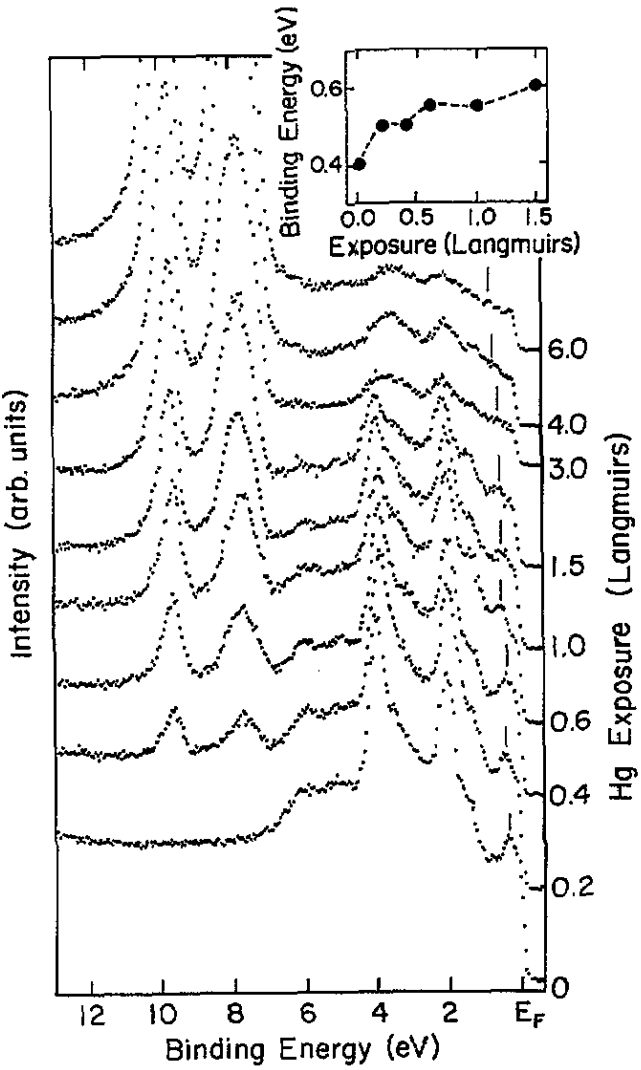

Figure 5. The photoemission spectra for Hg submonolayer coverages on W(110) at normal emission. 40 eV p-polarized light was used. The binding-energy changes of two W(110) surface states just below E_F as functions of Hg coverage are shown in the inset.

becomes increasingly well resolved with increasing coverage, particularly for more than one monolayer, and the binding energy decreases with coverage. This feature has also been observed for Hg on Cu(100) [3], Ag(100) [35], $Cu_3Au(100)$ [46], Ni(111) [2] and W(100) [42] and is a consequence of a band separated from the degenerate symmetry $5d_{5/2}$ levels at $\overline{\Gamma}$ as result of orbital overlap between adjacent adatoms, and intraatomic s-to-d orbital hybridization [24,46,47], as discussed in detail elsewhere [3,4,35,38,46,47]. The increasing intensity of this feature relative to other 5d features with increasing s-polarization suggests that the band is largely of d_{xz} and d_{yz} character rather than $d_{3z^2-r^2}$. This symmetry assignment is consistent with Hg on many other surfaces [3,35,46].

By fitting to the intense $5d_{5/2}$ features using Gaussian functions, we found that there is

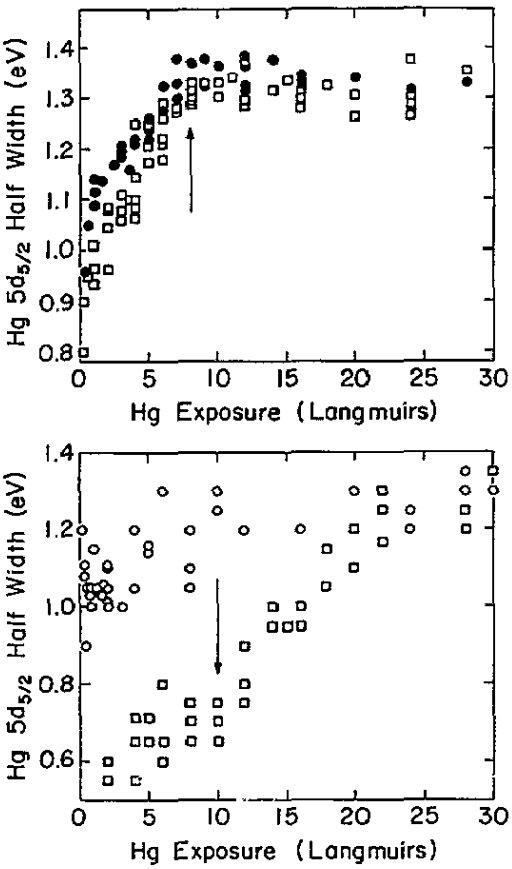

Figure 6. The Hg $5d_{5/2}$ photoemission half width. The data for Hg on W(110) are shown for s-polarized light (□) and p-polarized light (●) as a function of Hg exposure (and coverage) in the top panel. The Hg $5d_{5/2}$ width on Cu(100) (□) and Si(111) (○) as a function of exposure is shown in the bottom panel [3, 4]. The arrows indicate completion of one monolayer for Hg on W(110) and Cu(100) at 200 K.

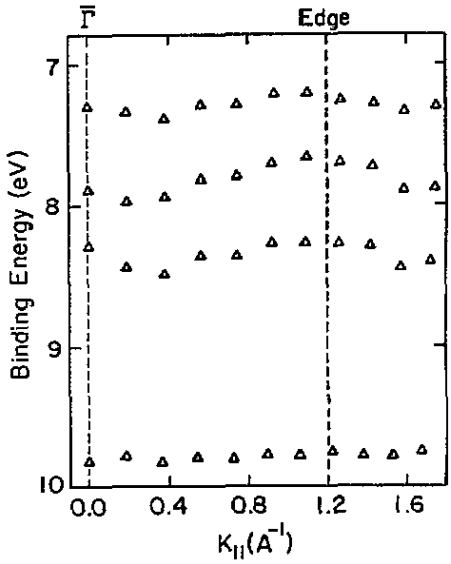

Figure 7. The experimental 5d band structures of one monolayer (8 L) Hg on W(110) determined by 40 eV s-polarized light. The dispersion is along $\overline{\Gamma N}$ of the clean W(110) Brillouin zone.

another Hg-induced feature at binding energy of about 8.3±0.1 eV, locating at the higher-binding-energy shoulder of Hg $5d_{5/2}$ states (figure 1). Comparing with $5d_{5/2}$ states, this feature has almost the same pattern of dispersion in k_{11} but a very weak intensity (figures 7 and 8). Unlike the 7.2 eV feature which is due to the hybridization of electron orbitals between adatoms and can only appear above certain coverage, the feature at 8.3 eV was observed even at low coverages. The binding energy and intensity of this feature are isotropic with respect to the light polarization. Therefore, it is likely that this feature is a result of crystal field splitting of 5d states [48].

Figures 7 and 8 show the experimental band dispersions of Hg 5d features for both one monolayer and two monolayers, respectively. Due to the mismatch between the overlayer and surface Brillouin zone, these two band mappings are not along the high-symmetry directions of the overlayer Brillouin zone but follow those of the W(110) Brillouin zone

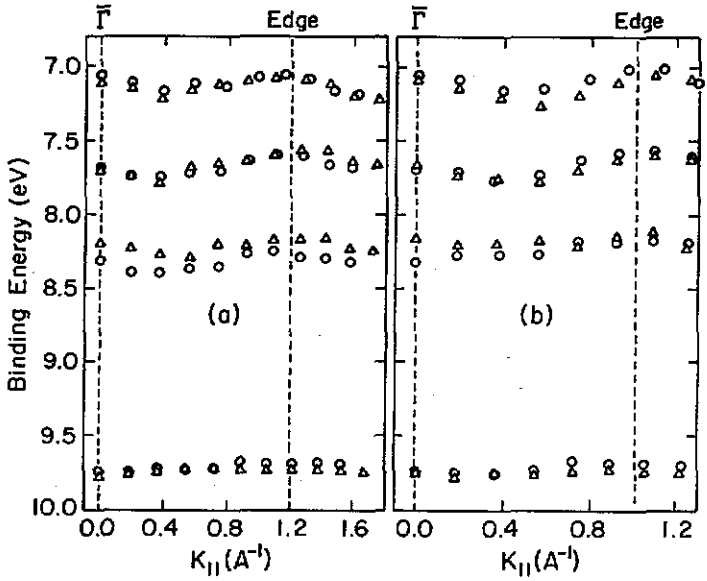

Figure 8. The experimental 5d band structures of two monolayers (16 L) Hg on W(110) determined by both 40 eV s-polarized light (△) and p-polarized light (○). The dispersion along $\bar{\Gamma}\bar{N}$ of the clean W(110) Brillouin zone is shown in (a) and that along $\bar{\Gamma}\bar{H}$ of the clean W(110) Brillouin zone is shown in (b).

high symmetry directions. The band mappings with respect to the overlayer Brillouin zone are as indicated in figure 3(c).

The Hg $5d_{3/2}$ feature with 9.7 eV binding energy did not disperse significantly with changing of emission angle nor there was a change in relative intensity. This is as observed for Hg overlayers on Ni(111) [2], Cu(100) [3] and Ag(100) [35, 38]. The Hg $5d_{5/2}$ feature with 7.8 eV binding energy and the second feature with 7.2 eV binding energy at $\bar{\Gamma}$ have similar dispersion for both even and odd geometry. These results may be compared with the calculations of Jansen, *et al* [24], and while not identical, our two-dimensional band structure does resemble the calculated two-dimensional free-standing hexagonal Hg monolayer electronic structure. This supports the previously discussed postulate that that the Hg film on W(110) is like a free-standing overlayer (i.e. weak hybridization between the overlayer and substrate).

A qualitative indication of overlayer band-structure formation can be seen in the behaviour of the full width at half maximum of the Hg $5d_{5/2}$ core-level envelope since changes as a consequence of band structure at $\bar{\Gamma}$ (as seen in figure 6) affect the formation of the 7.2±0.1 eV band. The Hg $5d_{5/2}$ width changes from about 0.8 eV to about 1.4 eV with increasing coverage. The change of the width of Hg $5d_{5/2}$ with coverage for Hg on Cu(100) [3, 4] and Si(111) [4] has also been reproduced in figure 6. Though the coverages indicated for Hg on W(110) cannot be applied to Cu(100) and Si(111) due to different sticking coefficients, the behaviour of the various Hg $5d_{5/2}$ half widths is nonetheless clear. Both Hg on W(110) and Hg on Cu(100) [3, 4] exhibit atomic Hg 5d widths at low coverages and large widths with the development of the 5d band structure. Little change is observed with Hg on Si(111) due to the strong chemisorption of Hg as discussed in detail elsewhere [4]. This indicates that even for dilute Hg coverages on Cu(100) and

W(110), the Hg interaction with the substrate is weak.

6. Formation of Hg quantum well states

In order to study the valence electronic structure change of the Hg overlayers with its coverage, we plot the detailed evolution of photoemission features in the low-binding-energy range with different Hg coverages in figure 9. Comparing with the original spectra in figure 1, the spectra in figure 9 (for both s- and p-polarized light) have been normalized to see relative changes of intensities of these features. There are several new features showing up at different Hg coverages, especially above half a monolayer (4 langmuirs), in contrast with the attenuation of substrate features.

There is a feature observed at 6.6±0.1 eV binding energy for Hg coverage greater than 5–6 langmuirs (this feature can be seen clearly away from the normal emission even though the feature overlaps with the Hg $5d_{5/2}$ feature at $\overline{\Gamma}$, as seen in figure 10). The intensity of this feature increases with increasing Hg coverage in the submonolayer range, reaches its maximum at one monolayer (8 L) and then decreases with further adsorption of Hg (figure 11). With coverages greater than one monolayer, there are two other features observed at 1.95±0.1 eV and 5.0±0.1 eV binding energy at $\overline{\Gamma}$. The intensities of these two features increase simultaneously with increasing thickness of the overlayer (figure 11). These two features did not show up before the completion of the first monolayer adsorption. All three features do not disperse with the photon energy (or $k_\perp$, i.e., they are truly confined within the overlayer) but show similar and considerable dispersion with photoelectron emission angle (or k_{11}) shown in figures 10, 12 and 13.

Given the layer-by-layer growth of the overlayer, and the onset and intensity change of these three features, the 6.6 eV feature is the quantum-well state when the overlayer is only one Hg layer thick and the other two features are the quantum-well states when the Hg overlayer is a bilayer. Given the distinct binding energies, the parabolic dispersion ($E(k_{11}) = \hbar^2 k_{11}^2/2m^*$) of these bands, and the $k_\perp$ independence of their binding energies, as well as their energy positions located in the band-gap mismatch between W and Hg, we can identify these bands as Hg sp-like quantum-well states [49]. There are many reports of similar quantum-well states [50–52], for pure metallic overlayers.

Figure 12 shows the dispersions of these features for 16 langmuir adsorption of Hg on W(110) at 200 K. The coexistence of these features is likely because the Hg overlayer corresponding to 16 langmuir exposure is not exactly two complete monolayers thick, i.e., the overlayer has one complete first layer and an incomplete second layer (two-dimensional islands). This result can also be seen from the intensity changes of these states with increasing coverage since the intensities of 1.95 eV and 5.0 eV quantum well states do not reach their maxima at 16 langmuirs. Figure 13 shows the dispersion of these states for both even and odd geometry with different Hg exposures. Both the 6.6 eV monolayer quantum-well state and the two bilayer quantum-well states (1.95 eV and 5.0 eV) have dispersion that is perfectly parabolic. Using least-squares fitting, we find that the in-plane effective masses of these states are close: $0.98m_e$ for the 6.6 eV feature, $1.06m_e$ for the 5.0 eV state, and $1.12m_e$ for the 1.95 eV feature, for the dispersion along $\overline{\Gamma N}$ of the clean W(110). This is reasonable since these quantum-well states are all related to the Hg bulk sp band [49].

Quantum well states are quantized electronic states of quasifree electrons confined within a thin slab and they are really characteristic of the overlayer. These quantum-well states can appear only when there are enough delocalized electrons in the slab. The onset of quantum-well states requires the onset of the metallicity of overlayer. It is clear that the

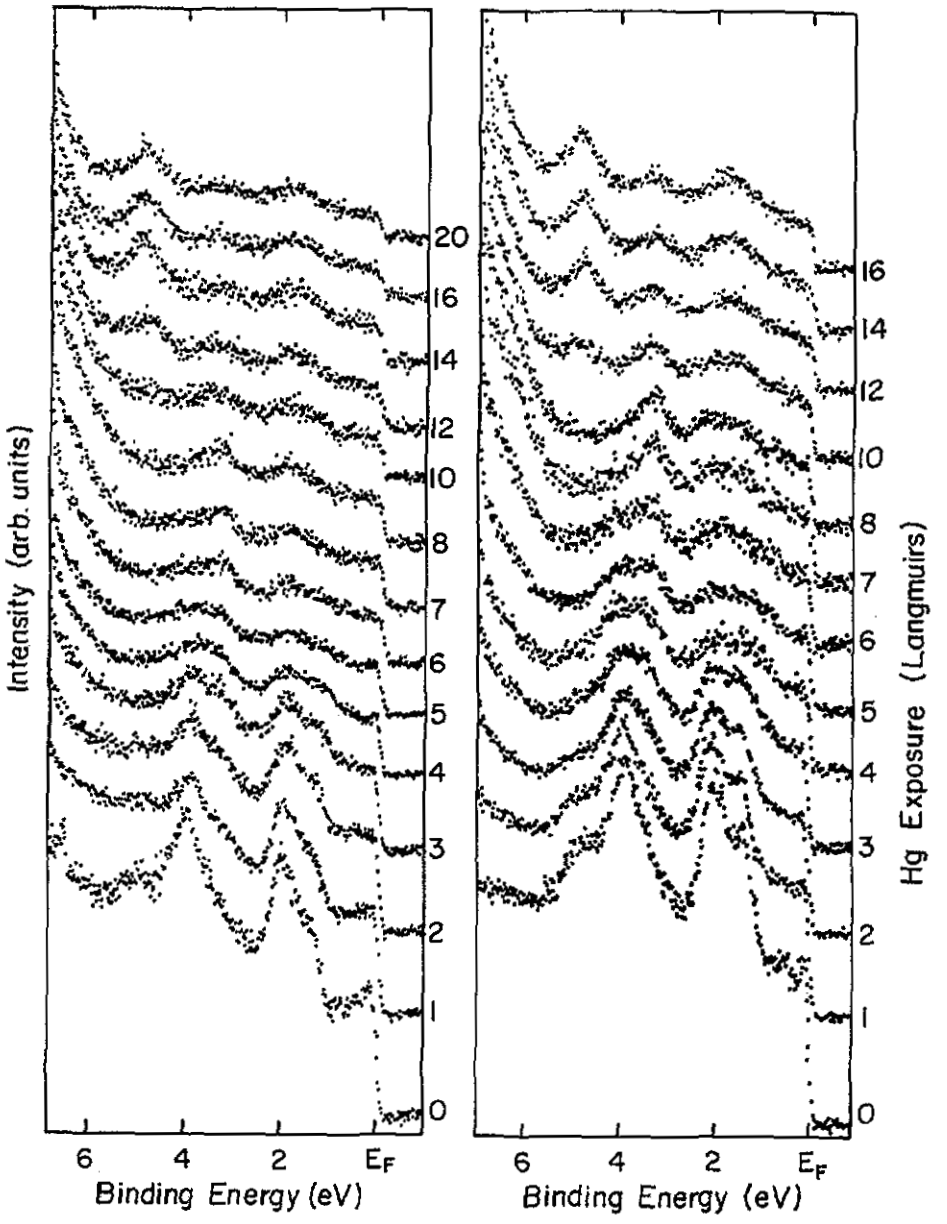

Figure 9. The valence-band photoemission spectra with different coverages of Hg on W(110) taken for both s-pofarized (a) and p-polarized (b) light. The photon energy used was 40 eV. All the binding energies are relative to the Fermi level.

band structure, in particular the quasifree electron quantum-well states, adopts a Brillouin zone of the overlayer lattice unperturbated by the substrate Brillouin zone. The Hg electronic structure is largely unhybridized with the W(110) band structure. This is true of the Hg overlayer throughout all stages leading to the development of the highly dispersive band structure. As noted in the previous section, there are similarities between the band structure

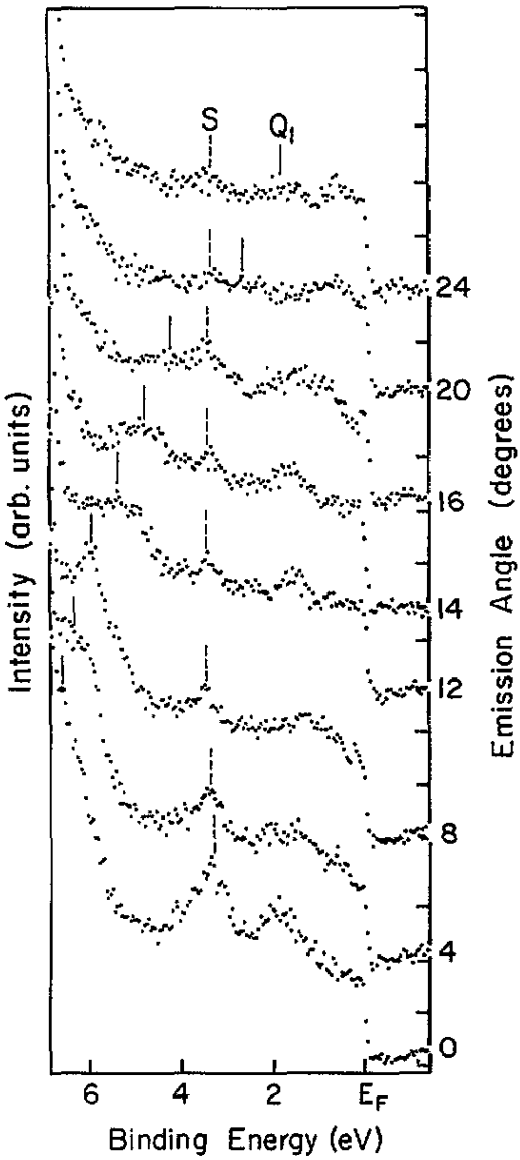

Figure 10. The photoemission spectra of 8 langmuirs Hg on W(110) with different emission angles along $\overline{\Gamma N}$ of the clean W(110) Brillouin zone. The quantum-well state Q and the interface/surface state S are indicated.

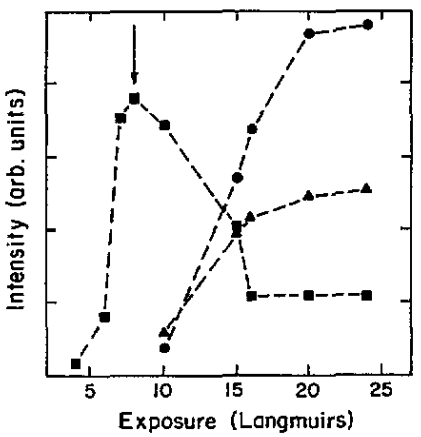

Figure 11. The intensity changes of the quantum-well states with increasing Hg exposure on W(110): ■, the state at 6.6 eV below E_F at $\overline{\Gamma}$; ●, the state at 5.0 eV below E_F at $\overline{\Gamma}$; and ▲, the state at 1.95 eV below E_F at $\overline{\Gamma}$. The photon energy used was 40 eV. The data correspond to the 4° off-normal photoemission spectra along $\overline{\Gamma N}$ of the clean W(110) Brillouin zone for p-polarized light. The arrow marks the completion of the first Hg monolayer adsorption on W(110). The dashed curves are just a guide.

of the Hg overlayer and the calculated band structure of a *free*-standing Hg film [24,47].

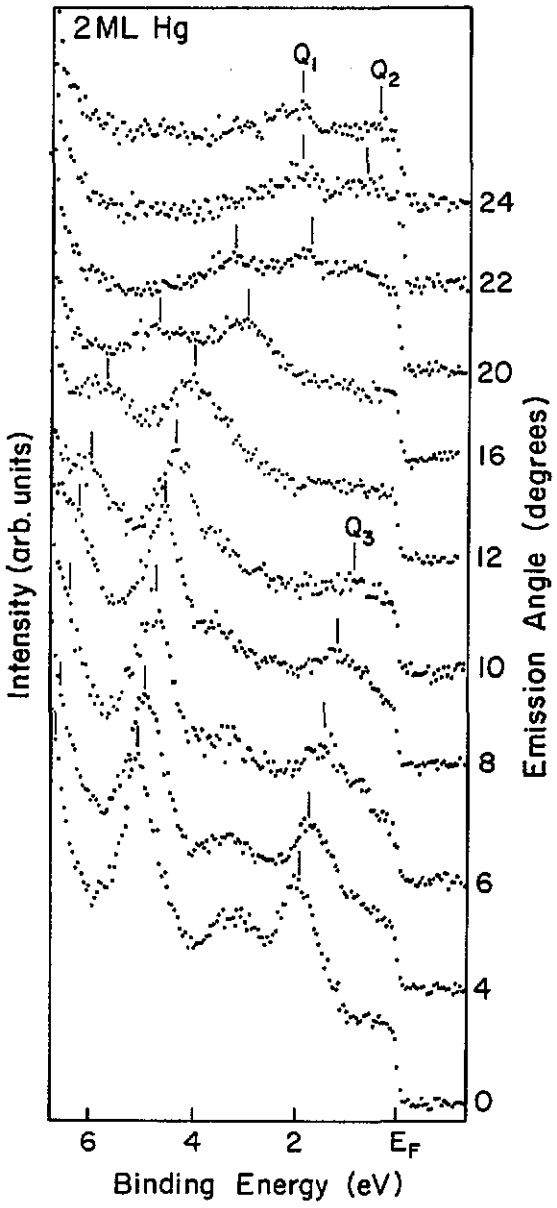

Figure 12. The normalized photoemission spectra of 16 langmuir Hg on W(110) with different emission angles along $\overline{\Gamma N}$ of the clean W(110) Brillouin zone. The corresponding quantum-well states are indicated. The photon energy used was 40 eV (p polarized).

Apart from these quantum-well states, there is a broad feature with a binding energy of 3.40±0.1 eV at $\overline{\Gamma}$ for about half a monolayer Hg coverage as seen in figures 5 and 9. The binding energy of the feature shifts to 3.25±0.1 eV after about a bilayer adsorption. This feature attains its maximum intensity at about one monolayer (6–8 langmuirs), then attenuates slowly with further Hg adsorption (figure 9), and the intensity of this feature increases with increasing p polarization of the incident light (figure 9). The feature has

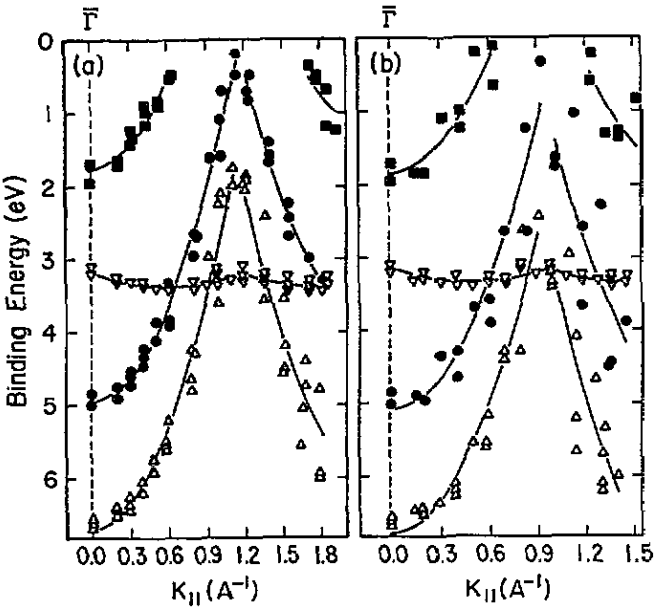

Figure 13. The Hg-induced quantum-well states and interface resonance feature dispersions (a) along $\overline{\Gamma N}$ of the clean W(110) Brillouin zone and (b) along $\overline{\Gamma H}$ of the clean W(110) Brillouin zone. The 6.6 eV (at $\bar{\Gamma}$) is the quantum-well state of one monolayer Hg, and the other two states (5.0 eV and 1.95 eV at $\bar{\Gamma}$) are the quantum states of the Hg bilayer. The photon energy used was 40 eV (p polarized). The solid curves are fits to the data.

a very small dispersion as seen in figures 10 and 12, but does not disperse as a function of photon energy. Therefore we can assign the feature as an interface/surface state or resonance, even though a further study is required.

7. Non-metal to metal transition

Only one kind of LEED pattern for the Hg overlayer on W(110) was observed at 200 K for several monolayers, thus formation of two-dimensional Hg islands occurs at submonolayer coverage [1]. When the surface bonding between overlayer and substrate is relatively weak, the overlayer exhibits quasifree-standing overlayer electronic properties as noted above and elsewhere [47] and undergoes a metallization process or non-metal-to-metal transition due to the effect of dimensionality (or the size of the islands) [1, 24, 22, 53]. This transition can now be compared with free clusters.

There are several methods to probe the metallicity of an overlayer or a thin film. Recently, Schad *et al* [22], using the traditional approach, measured the conductivity as function of the thickness and the temperature for Ag thin films on Si(111) and observed that films thinner than five monolayers are non-metallic (semiconducting). Whitman *et al* [16], using STM spectroscopy, and DiNardo *et al* [13], using the combination of photoemission and inverse photoemission, observed a gap at the Fermi energy for all Cs coverages less than one monolayer on GaAs(110). For metal overlayers on metal substrates these techniques will not work due to the metallic properties of the substrate. We have chosen to employ

two different experimental measures of metallicity. One indicator of the non-metal to metal transition is the width of the $5d_{5/2}$ shallow core level and the other measure is the change in the 5d→ ϵf resonance in CIS.

The non-metal-to-metal transition in the overlayer can be related to the electron localization–delocalization change or the change of the itinerant electron density in the overlayer. The change of the itinerant electron density is reflected by the change of the screening of the photoholes in the photoemission process and as discussed previously [1,3,4,54], resonance photoemission can be employed to observe this kind of relative change of the screening effect. With increasing metallicity of the overlayer or the density of itinerant electrons, it will increase the screening and decrease the interaction between the photohole and outgoing electron such that there is a shift of the resonant cross-section maximum in resonant photoemission to higher photon energy for the Hg 5d-to-ϵf resonance. The increased screening will decrease the core-hole lifetime as well so that the resonant photoemission peak is broader in CIS.

The CIS resonant photoemission spectra for the Hg overlayer are shown in figures 14 and 15, for s-polarized and p-polarized light, respectively. The data are shown for the initial states just below the Fermi level, and similar results were obtained with other initial states including the Hg 5d core levels. The spectra and the resonance intensity changes with coverage were obtained after normalization by photon flux and subtraction by the contribution from the substrate. After 3 L exposure of Hg, for both s- and p-polarized light, there are two weak and broad resonant enhancement features at about 47 eV and 60 eV in photon energy. For the 47 eV resonance peak, the intensity increases with increasing Hg coverage, especially at 3–10 langmuirs exposure, and reaches a maximum well after the completion of adsorption of the first monolayer. However, the photon energy of this resonance at 47 eV appears to be largely coverage independent (figures 14 and 15). On the other hand, the 60 eV resonance feature, which is due to 5d-to-ϵf excitation [3], shifts the resonance photon energy dramatically from 56 to 62 eV in the low-coverage range, and then becomes broader with increasing coverage. We assign this broad feature as the Hg 5d-to-ϵf resonance [1,3,4].

The shift of this 5d-to-ϵf resonance for the 5d/6s initial-state photoelectrons is an obvious indication of increased screening of the photoholes or increasing itinerant electron density in the overlayer [1]. For the coverages between 3 and 8 langmuirs (or $\frac{1}{3}$–1 monolayer), the resonance intensity increases gradually and reaches a maximum at about one monolayer. This indicates that the film is increasingly but not fully metallic [1]. For exposure greater than 8 langmuirs, the resonance energy is coverage independent (from both Fermi level initial states as shown in figures 14 and 15 and for the $5d_{5/2}$ initial state). The resonance intensity for 5d-to-ϵf resonance declines following completion of a monolayer. These results suggest that for 8 langmuirs or more, the overlayer is totally metallic. Furthermore, there exists a gradual non-metal-to-metal transition in the submonolayer range.

While resonance at 60 eV photon energy could be a result of the Hg 5p-to-5d/6s Coster–Kronig transition in the metallic Hg overlayer, this is not the case. For this resonance to be a Coster–Kronig resonance, an unoccupied state must be filled by a core-excited electron in the resonant photoemission process [55]. This intermediate excitation (followed by an Auger-like decay) can occur well below the threshold as a result of the unoccupied level being brought down in energy in the extreme screening limit [55,56]. A suitable 6s/6p state and 5d/6s states of the correct symmetry are predicted at k_{11}=0 in the hexagonal metallic Hg monolayer [24] and are observed as noted previously. The cross-section of this Coster–Kronig excitation could be increased by the existence of such a hybridization state during increasing metallicity of the overlayer. This kind of $5p_{3/2}$ → 5d/6s resonance has

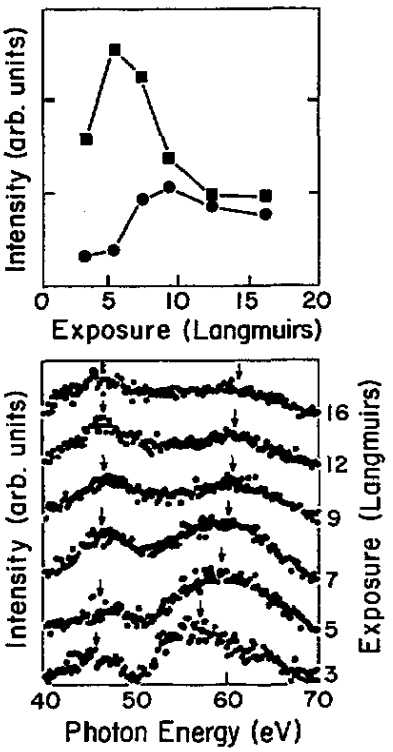

Figure 14. The Hg CIS photoemission spectra for Hg on W(110) taken by s-polarized light. The photoelectrons were collected in the normal direction from the initial states just below the Fermi energy. The 5d→ ϵf resonance intensity at about 60 eV with coverage ■ and the resonance at 47 eV with coverage ● are shown at the top of the figure. The shift in the 5d→ ϵf resonance with coverage is indicated by the arrows.

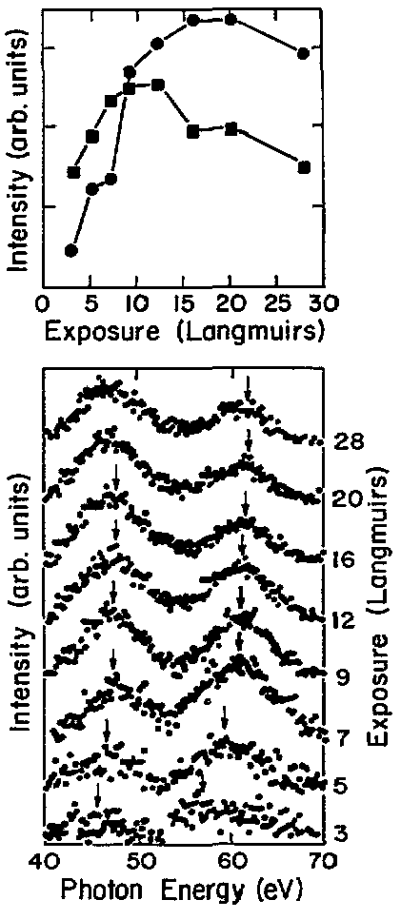

Figure 15. The Hg CIS photoemission spectra for Hg on W(110) taken by p-polarized light. The photoelectrons were collected in the normal direction from the initial states just below the Fermi energy. The 5d→ ϵf resonance intensity at about 60 eV with coverage ■ and the resonance at 47 eV with coverage ● are shown at the top of the figure. The shift in the 5d→ ϵf resonance with coverage is indicated by the arrows.

been previously observed at 60 eV (5 eV below the 65 eV threshold for this 5p-to-5d/6s resonance [56]), but the width of that resonance (only 1–2 eV) is much smaller than the width we observed for the resonance in the Hg/W(110) system, and appears together with 5d to ϵf resonance. A Coster–Kronig transition resonance should not exhibit a resonance photon-energy dependence upon coverage as is observed between 3 and 8 langmuirs exposure. The resonance at 60 eV is therefore due to a 5d → ϵf excitation, not a 5p → 5d/6s Coster–Kronig transition.

There are several possible origins for the appearance of the weak resonance feature at 47 eV. One possible mechanism for the 47 eV resonance is that it could be an Hg resonance (like the 5d → ϵf resonance) attributable to a very non-metallic overlayer [3, 4]. This assignment requires a non-metallic first Hg monolayer and then at least the formation

of a partial non-metallic Hg overlayer on the first metallic Hg layer (following completion of the first Hg layer), since the intensity of this resonance increases beyond the formation of the first monolayer and reaches a maximum well into adsorption of the second layer. This assignment is inconsistent with the band-structure results (including the onset of the quantum-well states in the submonolayer range) and the assignment of the 60 eV resonance. A partial non-metallic overlayer on the first metallic first layer requires three-dimensional island formation as opposed to the observed layer-by-layer growth mode. Furthermore, this assignment is inconsistent with the work-function change, and the existing thermal desorption studies [36, 57]. Assigning this feature to $5p_{3/2}$-to-5d/6s resonance cannot be supported by our data. This resonance at 47 eV photon energy is 18 eV below the threshold. The photon energy half width of nearly 7 eV is also difficult to reconcile with a single-state resonance brought below the threshold by Coulomb interaction since such effects, seen before with Hg, result in a resonance with width 1–2 eV [56]. Photoelectron diffraction effects can create very weak variation in the CIS spectra that may appear to resemble a resonance. Diffraction effects can be excluded because of the dramatic light polarization effects observed in this resonance intensity and because the observed resonance is fixed in photon energy for several different initial states—not fixed in kinetic energy.

One of the important observations that assists in explaining this feature is the anisotropy of the resonance intensity for different light polarizations. The 47 eV resonance relative to the 60 eV one is strongly enhanced in p-polarized light (figures 14 and 15). In a highly metallic Hg overlayer, the 5d-to-ϵf resonance can be strongly affected by the Fermi electron sea [55] and light polarization effects can be expected. The excitation of inverted virtual (plasmon-like) multimodes in the $5d \rightarrow \epsilon f$ resonant process can result in a second resonance, so the photon energy difference between the two resonances is approximately equal to the 6sp bandwidth. Alternatively, the W $5p_{1/2}$ level at 45.3 eV binding energy can result in the resonance that can be reconciled with our data if the excitation is extraatomic. Since extraatomic excitations for the W $5p_{1/2}$ that couple with 5d/6s unoccupied states of Hg involve dipoles with moment normal to the surface, this resonance is likely to be highly p polarized. Given the light-polarization dependence of this resonance and noting that these CIS spectra are taken for $k_{11}=0$, we suggest that the 47 eV resonance is a result of the metallic character of the Hg overlayer.

The Hg 5d shallow-core-level photoemission full width at half maximum changes as a result of increasing Hg coverage as noted previously. The increasing $5d_{5/2}$ width is related to the Hückel-like orbital overlap and hybridization between adjacent adatoms as noted previously [1–4, 46]. This indication of band-structure formation also indicates that the transition to a fully metallic overlayer is gradual.

The evolution of Hg 5d shallow core photoemission widths, the appearance of quantum-well states, and the development of two weak resonances in CIS all consistently suggest that the Hg overlayer undergoes a gradual non-metal to metal transition in the submonolayer range. The CIS feature at 56–62 eV is a good indicator of the gradual onset of metallic behaviour (at 3–8 L) and if also indicative of the increasingly metallic behaviour with Hg coverage between 3 and 10 L. The appearance of quantum-well states confirms the complete metallicity at 8–10 langmuirs adsorption. These results are also consistent with indications of metallicity found for Hg overlayers on other surfaces [1, 3].

The overlayer structure, the adatom coordination, and the surface bonding are believed to be major factors in determining the changes of overlayer electronic properties, such as the non-metal-to-metal transition [3, 4, 24]. For Hg on Cu(100) at 200 K, the non-metallic behaviour of the overlayer (at the first monolayer, or less than 10 langmuirs) is attributable to low average coordination number ($\leqslant 5$) and the large lattice constant (>3 AA) [3]. The

change to metallic behaviour with the adsorption of the second layer of Hg on Cu(100) is related to the increase of Hg coordination [3]. Similar behaviour was observed for the Hg/Ni(111) system [2, 47]. For Hg on Si(111), the metallic character (even at low coverage) is due to the strong bonds between Hg and the Si(111) substrate or the formation of mercury silicide.

Hg on W(110), as compared with Hg on Cu(100), exhibits a non-metal to metal transition of the Hg overlayer at much lower coverage. We postulate that two-dimensional island formation is responsible for the gradual non-metal-to-metal transition for Hg on W(110) at 200 K [1]. Consistent with the LEED result, such 2D islands would have to have a distorted hexagonal structure (at least in principle) with a sufficiently small lattice constant to obtain the necessary coordination for metallicity in the absence of strong bonding [4], though recently it has been suggested that the same may be true of a square adlayer structure [47]. The edges of these 2D islands would reduce the average coordination number, so an adlayer of very small islands as occurs at dilute coverage is still non-metallic as is the case with many submonolayer divalent adlayers (Hg on Cu(100) [3], Hg and Ba on Ni(111) [2, 3]). With increasing coverage, the gradual increase of island size is accompanied by the gradual increase of average adatom coordination number as the islands are increasingly less dominated by edges, the LEED pattern observed corresponding to the hexagonal structure. This overlayer structure is also consistent with the calculated lattice constant of 3.0 Å for the onset of the metallic-behaviour free standing Hg monolayer [24] and the structural phase transition observed for Hg on Ni(111) [24]. Furthermore, such island formation is also consistent with the substantial mobility of divalent metals on W(110) [58] and the large pairwise lateral interaction for Hg on W(100) [26].

According to Rademann *et al* coordination numbers between six and 10–11 ensure some metallic character but this represents for the free clusters a gradual transition region in metallicity [28, 29]. As the gradual change of free-cluster ionization potential is an indicator of the gradual non-metal-to-metal transition of the cluster (as shown in figure 16), the gradual changes of the CIS resonance peak positions are also indicative of gradual changes in the Hg overlayer metallicity. On the other hand, the correlation between the evolution of CIS resonance and band structure (including 5d width and quantum-well states) is undoubtedly because a more established band structure develops as the two-dimensional island size grows [59], which results in a better screening of the photoholes.

If the structure of 2D islands in dilute coverage were the noted distorted hexagonal structure, then for very small islands the average coordination number would have to be far less than six, corresponding to non-metallic free Hg clusters and Hg on Cu(100) [3] islands. With a gradual increase in average coordination (and island size), a large island of a hexagonal adlayer will have an average coordination number between six and seven (six from the adlayer and one from the substrate atom), which is consistent with a metallic coordination. This kind of gradual evolution of adlayer metallicity is very similar to the evolution of metallicity of free Hg clusters and of some other metal clusters [28–32]. The average coordination number of Hg clusters changes with change of size so the metallicity of clusters also changes with the cluster size.

From our data, we cannot exclude the possibility that the non-metal-to-metal transition could be due to the percolation of islands even though we have assumed (as before [1]) that the transition is the result of the gradual size change (or scaling) of individual islands. In order to confirm whether the non-metal-to-metal transition in two-dimensional islands that is determined by adatom average coordination is directly comparable to that in free clusters, further detailed studies of the two-dimensional island growth of the Hg overlayer by STM or even atom beam scattering [60] are essential. Adsorption of divalent metal overlayers

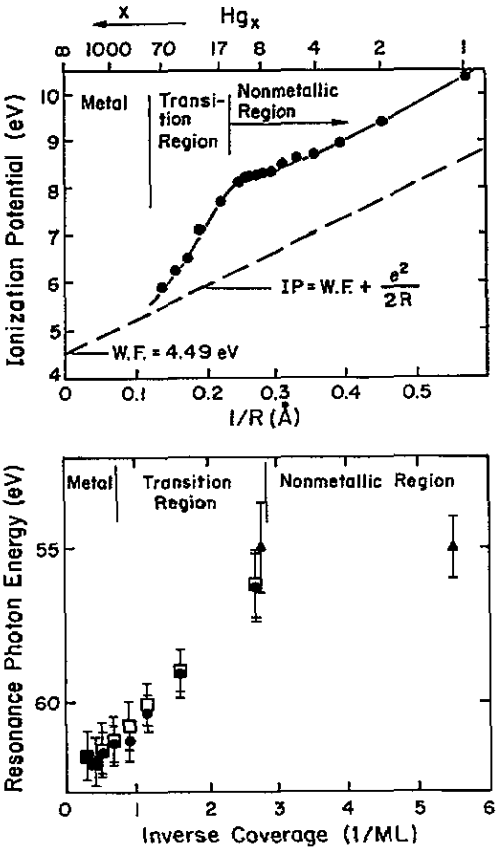

Figure 16. The comparison for the gradual non-metal-to-metal transition between the Hg free clusters and the Hg overlayers on W(110). The ionization-potential change of free Hg clusters as function of the cluster size is shown on the left of the figure [28]. The resonance-energy change in CIS for the 5d→ εf excitation of the Hg overlayer as function of inverse coverage is shown on the right of the figure, for both s- □ and p-polarized ● light. The data for the Hg overlayer on Cu(100) (at dilute Hg coverages only) with p-polarized light is shown by ▲.

on close-packed surfaces, such as Be(0001), Mo(110), and W(110), may exhibit similar behaviours as described above and can also provide an additional test of models that relate the average coordination number of adatoms in surface islands to metallicity.

8. Summary

In the submonolayer range, the Hg overlayer exhibits a non-metal to metal transition. A gradual evolution from localized to delocalized states of the valence electrons was observed, consistent with the formation of an overlayer band structure (in particular there is a change of Hg 5d feature widths), the onset of quantum-well states, and the evolution of CIS resonance features due to the change of screening effect to core excitons in resonant photoemission spectroscopy.

The formation of two-dimensional islands and the gradual increase of their size, which results in a gradual increase of average adatom coordination with increasing coverage,

corresponds to the gradual increase of the overlayer metallicity. This kind of gradual non-metal-to-metal transition is very similar to that of free Hg clusters. This similarity can be explained as the same pattern of average coordination evolution of Hg atoms for both systems. The electronic structure of the Hg overlayer is only very weakly perturbed by the substrate, even after the onset of a metallic Hg band structure. This is consistent with theoretical models of closed-shell metal surfaces [23]. Once metallic Hg forms quantum-well states it in many respects resembles a free electron metal (though we do not typically consider Hg a free-electron system).

Acknowledgments

The authors would like to thank Professor M Onellion, Professor E W Plummer, Professor Klaus Rademann, and Professor Changfeng Chen for a number of helpful discussions. The authors would like to thank Dr P S Mangat and Synchrotron Radiation Center staff for their technical help. This work was supported by the NSF through grant No DMR-92-21655 and the Synchrotron Radiation Center in Stoughton, WI is also supported by the NSF.

References

[1] Jiandi Zhang, Dongqi Li and Dowben P A 1993 *Phys. Lett.* **173A** 183
[2] Singh N K and Jones R G 1988 *Chem. Phys. Lett.* **155** 463 (1988); 1990 *Surf. Sci.* **232** 229, 243
[3] Dowben P A, LaGraffe D, Dongqi Li, Vidali G, Zhang L, Dottl L and Onellion M 1991 *Phys. Rev.* B **43** 10677
[4] Dongqi Li, Jiandi Zhang, Sunwoo Lee and Dowben P A 1991 *Phys. Rev.* B **45** 11876
[5] Gorodesky D A and Melnick Yu P 1977 *Surf. Sci.* **62** 647
[6] Katrich G A, Kimov V V and Yakovkin I N 1992 *Ukr. J. Phys.* **37** 429
[7] Dowben P A and LaGraffe D 1990 *Phys. Lett.* **144A** 193
[8] Binns C, Norris C and Gurman S A 1983 *J. Phys. C: Solid State Phys.* **16** 417
Binns C, Barthés-Labrousse M G and Norris C 1984 *J. Phys. C: Solid State Phys.* **17** 1465
Binns C and Norris C 1991 *J. Phys.: Condens. Matter* **3** 5425
[9] Plummer E W 1992 private communication; Watson G M, Bruwyler B and Plummer E W *Phys. Rev. Lett.* at press
Watson G M 1992 *PhD Thesis* University of Pennsylvania
[10] Plummer E W and Dowben P A 1993 *Prog. Surf. Sci.* **42** 201
[11] Dowben P A and Plummer E W *Rev. Mod. Phys.* in preparation
[12] Batra I P, Tekman E and Ciraci S 1991 *Prog. Surf. Sci.* **36** 289
[13] DiNardo N J, Maeda Wong T and Plummer E W 1990 *Phys. Rev. Lett.* **65** 2177
Maeda Wong T, Heskett D, DiNardo N J and Plummer E W *Surf. Sci.* **208** L1
[14] Arekat S, Kevan S D and Richmond G L 1993 *Europhys. Lett.* **22** 377
[15] Aruga T, Tochihara H and Murata Y 1984 *Phys. Rev. Lett.* **53** 372
[16] Whitman L J, Stroscio J A, Dragoset R A and Celotta R J 1991 *Phys. Rev.* B **44** 5951
[17] Jeon D, Hashizume T, Sakurai T and Wills R F 1992 *Phys. Rev. Lett.* **69** 1419
[18] Johansson L S O and Reihl B 1991 *Phys. Rev. Lett.* **67** 2191
Magnusson K O, Wiklund S, Duddle R and Reihl B 1991 *Phys. Rev.* B **44** 5657
Hebenstreit J, Heinemann M and Scheffler M 1991 *Phys. Rev. Lett.* **67** 1031
[19] Stiles K and Kahn A 1988 *Phys. Rev. Lett.* **60** 440
[20] Ludeke R, Jezequel G and Jaleb-Ibrahimi A 1988 *Phys. Rev. Lett.* **61** 601
[21 Riffe D M, Weitheim G K, Rowe J E and Citrin P H 1992 *Phys. Rev. Lett.* **45** 3532
[22] Schad R, Heun S, Heidenblut T and Henzler M 1992 *Phys. Rev.* B **45** 11430
[23] Miedema A R and Dorleijn J W F 1981 *Philos. Mag.* B **43** 251
[24] Jansen H J F, Freeman A J, Weinert M and Wimmer E 1983 *Phys. Rev.* B **28** 593
[25] Kime Y J, Jiandi Zhang and Dowben P A 1992 *Surf. Sci.* **268** 98

[26] Jones R G and Perry D L 1978 *Surf. Sci.* **71** 59; 1979 *Surf. Sci.* **82** 40
[27] Jones R G and Tong A W-L 1987 *Surf. Sci.* **188** 87
[28] Rademann K, Kaiser B, Even U and Hensel F 1987 *Phys. Rev. Lett.* **59** 2319; 1989 *Z. Phys.* D **12** 431
Kaiser B and Rademann K 1992 *Phys. Rev. Lett.* **69** 3208
[29] Rademann K 1989 *Ber. Bunsenges. Phys. Chem.* **93** 653
[30] Bréchignac C, Broyer M, Cahuzac Ph, Delacretaz G, Labastie P, Wolfe J P and Wöste L 1988 *Phys. Rev. Lett.* **66** 265
[31] Jortner J 1992 *Z. Phys.* D **24** 247 and references therein
Meiwes-Broer K H 1992 *Appl. Phys.* A **55** 430
[32] Pastor G M, Sampfli P and Bennemann K H 1988 *Europhys. Lett.* **7** 419
Garcia M E, Pastor G M and Bennemann K H 1991 *Phys. Rev. Lett.* **67** 1142
Stampfli P and Bennemann K H 1992 *Phys. Rev. Lett.* **69** 347
Aligia A A A, Garcia M E and Bennemann K H 1993 *Europhys. Lett.* **7** 419
[33] Dowben P A, LaGraffe D and Onellion M 1989 *J. Phys.: Condens. Matter* **1** 6571
[34] Horlacher-Smith A, Barker R A and Estrup P J 1984 *Surf. Sci.* **136** 329
Roelofs L D, Chung J W, Ying S C and Estrup P J 1986 *Phys. Rev.* B **33** 6537
[35] Dowben P A, Kime Y J, Varma S, Onellion M and Erskine J L 1987 *Phys. Rev.* B **36** 2519
Dowben P A, Onellion M and Kime Y J 1988 *Scanning Microsc.* **2** 177
[36] Zhao Y B and Gomer R 1992 *Surf. Sci.* **271** 85
[37] Li W, Jingsu Lin, Karimi M, Dowben P A and Vidali G 1992 *Phys. Rev.* B **45** 3708
[38] Onellion M, Erskine J L, Kime Y J, Varma S and Dowben P A 1986 *Phys. Rev.* B **33** 8833
[39] Powell C J 1974 *Surf. Sci.* **44** 29
Penn D R 1976 *J. Electron. Spectrosc. Relat. Phenom.* **9** 29
Seah M P and Dench W A 1979 *Surf. Interface. Anal.* **1** 2
[40] Estrup P J and McRae E G 1971 *Surf. Sci.* **25** 1
[41] Holmers M W, King D A and Inglesfield J E 1979 *Phys. Rev. Lett.* **42** 394
Gaylord R H and Kevan S D 1987 *Phys. Rev.* B **36** 9337
Gaylord R H, Jeong K H and Kevan S D 1989 *Phys. Rev. Lett.* **64** 2036
[42] Egelhoff W F Jr, Peny D L and Linnett J W 1976 *Surf. Sci.* **54** 670
[43] Soukiassian P, Riwan R, Lecante J, Wimmer E, Chubb S R and Freeman A J 1985 *Phys. Rev.* B **31** 4911
Soukiassian P, Riwan R and Borensztein Y 1979 *Solid State Commun.* **44** 1375
[44] Lindgren S A and Wallden L 1979 *Chem. Phys. Lett.* **64** 239
[45] Wimmer E, Freeman A J, Weinert M, Krakauer H, Hiskes J R and Karo A M 1982 *Phys. Rev. Lett.* **48** 1128
Wimmer C E, Freeman A J, Hiskes J R and Karo A M 1983 *Phys. Rev.* B **28** 3074
[46] Onellion M, Kime Y J, Dowben P A and Tache N 1987 *J. Phys. C: Solid State Phys.* **20** L633
Dowben P A, Varma S, Kime Y J, Mueller D R and Onellion M 1988 *Z. Phys.* B **73** 247
[47] Singh N K, Dale P, Bullett D and Jones R G 1993 *Surf. Sci.* **294** 333
[48] Herbst J F 1977 *Phys. Rev.* B **15** 3720
Ishi S and Ohno Y 1983 *Surf. Sci.* **133** L465 and reference therein
[49] Dowben P A, Jiandi Zhang and Dongqi Li in preparation
[50] Miller T, Samsavar A, Franklin G E and Chiang T-C 1988 *Phys. Rev. Lett.* **61** 1404
Mueller M A, Miller T and Chiang T-C 1990 *Phys. Rev.* B **41** 5214
Mueller M A, Samsavar A, Miller T and Chiang T-C 1989 *Phys. Rev.* B **40** 5845
[51] Himpsel F J 1991 *Phys. Rev.* B **44** 5966
Ortega J E and Himpsel F J 1992 *Phys. Rev. Lett.* **69** 844
Ortega J E, Himpsel F J, Mankey G J and Wills R F 1993 *Phys. Rev.* B **47** 1540
[52] Lindgren S Å and Wallden L 1988 *Phys. Rev. Lett.* **61** 2894; 1988 *Phys. Rev.* B **38** 3060; 1987 *Phys. Rev. Lett.* **59** 3003
Loly P D and Pendry J B 1983 *J. Phys. C: Solid State Phys.* **16** 423
Brookes N B, Chang Y and Johnson P D 1991 *Phys. Rev. Lett.* **67** 354
Jalochowski M, Knoppe H, Lillenkamp G and Bauer E 1992 *Phys. Rev.* B **46** 4693
[53] Hodgkinson R J 1990 *J. Phys.: Condens. Matter* **2** 6563
Chaudhari P, Habermever H-U and Muekawa S 1985 *Phys. Rev. Lett.* **55** 430
Octavio M, Gutierrez G and Aponte J 1987 *Phys. Rev.* B **36** 2461
Cheriet L, Helbig H H and Arajs S 1989 *Phys. Rev.* B **39** 9828
Lourens J A J, Arajs S, Helbig S F, Mehanna E-S A and Cheriet L 1988 *Phys. Rev.* B **37** 5423
Fisher G, Hoffmann H and Vancea J 1980 *Phys. Rev.* B **22** 6065

[54] Schwinger J 1948 *Phys. Rev.* **73** 407
B'ethe H A 1949 *Phys. Rev.* **76** 38; 1987 *Giant Resonances in Atoms, Molecules and Solids (NATO ASI Series)* ed J P Connerade, J M Estera and R C Karnatak (New York: Plenum)
[55] Wendin G 1981 *Breakdown of the One-Electron Pictures in Photoelectron Spectra (Structure and Bonding)* vol 45, (Berlin: Springer)
[56] Varma S, Kime Y J, Dowben P A, Onellion M and Erskine J L 1986 *Phys. Lett.* **116A** 66
[57] Swanson L W, Stayer R W and Davis L E 1968 *Surf. Sci.* **9** 165
[58] Naumovets A G, Popavsky V V and Vedula Yu S 1988 *Surf. Sci.* **200** 231
[59] Sugano S 1991 *Microcluster Physics (Springer Series in Materials Science)* vol 20 (Berlin: Springer)
[60] Wei Li, Vidali G and Biham O 1993 *Phys. Rev.* B **48** 8336